Xiang *et al. Chem. Biol. Technol. Agric.* (2024) 11:39
https://doi.org/10.1186/s40538-024-00563-3

Chemical and Biological Technologies in Agriculture

RESEARCH

Open Access

Purification, structural characterization, and immunoregulatory activity of a polysaccharide from mulberry branch

Wei Xiang[1,2], Li Xu[3], Li Zheng[4], Qi-ao Zhang[3] and Xiaowen Shi[4*]

Abstract

In view of the fact that mulberry branch has not been effectively utilized and polysaccharide is one of the main active components in mulberry branch, this study aims to reveal the structure and immunomodulatory activity of its polysaccharide. A type of neutral polysaccharides, named mulberry branch polysaccharide-2 (MBP-2), was separated from mulberry branch using DEAE-52 and Sephadex G-100. As analyzed, they were mainly composed of glucose with a molecular weight of approximately 21.7 kDa. Methylation analysis demonstrated that MBP-2 primary contained a → 4)-*α*-D-Glc*p*-(1 → , *α*-D-Glc*p*-(1 → and → 4, 6)-*α*-D-Glc*p*-(1 → structure, which was validated by nuclear magnetic resonance (NMR). In addition, cellular experiments indicated that MBP-2 significantly enhanced the production of NO, TNF-α and IL-6 in RAW264.7 cells, unraveling the potential immunoregulatory activity of MBP-2. Further analysis showed that MBP-2 exerted their immunoregulatory activity mainly via binding with TLR4 to activate the downstream TRIF-dependent signaling pathways.

Highlights

1. A homopolysaccharide (MBP-2) was purified from mulberry branch;
2. This study first reported the glucan polysaccharides from mulberry branch;
3. MBP-2 had potent immunoregulatory activity;
4. MBP-2 exerted immunoregulatory activity via the TRIF-dependent signaling pathway.

Keywords Mulberry branch, Homopolysaccharide, Immunoregulatory activity, Toll-like receptor 4

*Correspondence:
Xiaowen Shi
xiaowenshi1990@zjxu.edu.cn
Full list of author information is available at the end of the article

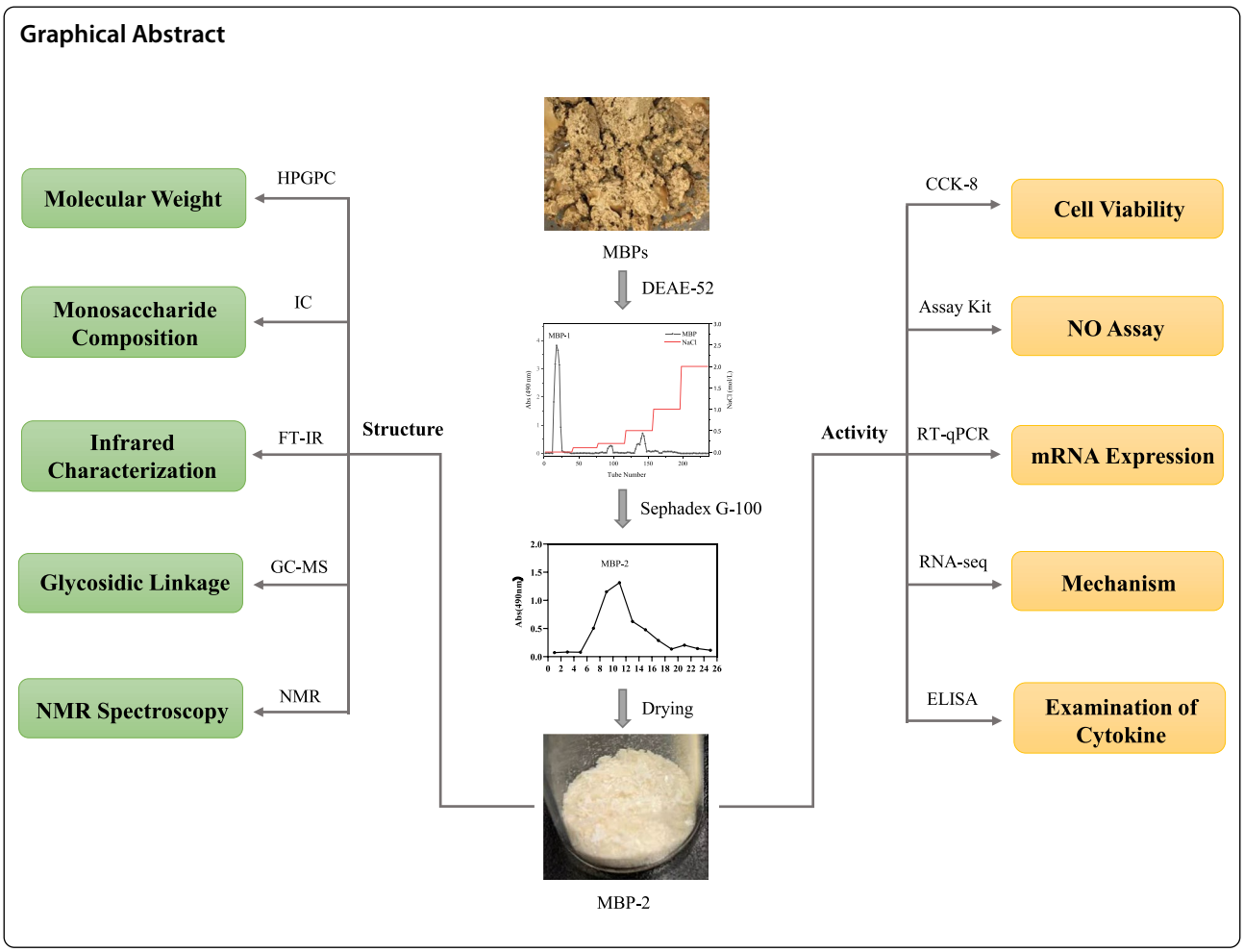

Introduction

Mulberry (*Morus* spp.) is a kind of cash crop widely planted in Asia [1]. Mulberry branch (*Ramulus mori*), a by-product of mulberry tree, has not been effectively utilized at present [2]. Modern studies have reported that mulberry branch is rich in multiple chemical components, including polysaccharides [3], flavone [4], and alkaloids [1]. Jialing 20 is an artificial triploid mulberry variety widely planted in Southwest China. In previous studies, we analyzed the small molecular components of its branch extract [5] and identified its active components that inhibit α-glucosidase [6] and butyrylcholinesterase [7]. However, there are few reports on the structure and activity of its polysaccharide.

Polysaccharides are a class of complex carbohydrates with a large molecular weight [8]. They are an assembly of monosaccharides linked together by glycosidic linkages and are widely found in plants, animals and microorganisms [9]. It has been reported that mulberry leaf polysaccharides, mulberry fruit polysaccharides, mulberry branch polysaccharides, and mulberry root bark polysaccharides have a variety of biological activities, but most of the current evidence focuses on the antidiabetic activity of mulberry leaf polysaccharides and mulberry fruit polysaccharides [10, 11]. Mulberry branch polysaccharides (MBPs), as one of the main active ingredients in mulberry by-products, have preferable anti-tumor [12], antioxidant [13], and hypoglycemic [14] activities. However, its immunoregulatory activity is rarely reported.

Immunity is the capability of host to resist harmful microorganisms (viruses, bacteria, etc.). [15]. Human immunity is classically divided into innate and adaptive components, where macrophages play vital roles [16]. In response to a certain stimulus or damage, macrophages release a series of pro-inflammatory factors, such as nitric oxide (NO), tumor necrosis factor (TNF) -α, and interleukin (IL) -6, thereby regulating the immunity of the organism [17]. Native polysaccharides are commonly used as immunoregulators given their activity to activate macrophages and low toxicity [18].

The present study focused on Jialing 20 mulberry branch polysaccharide (MBP) to perform structural characterization and assessment for its potential immunoregulatory activity, so as to unravel more biological activity of MBP and help better utilize this biological resource.

Materials and methods

Materials and reagents

DEAE-52 and Sephadex G-100 were purchased from Yuanye Bio-Technology Co., Ltd. (Shanghai, China). Lipopolysaccharides (LPS), TAK-242 and C29 were purchased from MedChemExpress Co., Ltd. (Monmouth Junction, NJ, USA). Trifluoroacetic acid (TFA) was purchased from ANPEL Laboratory Technologies Lnc. (Shanghai, China). Monosaccharide standards (Arabinose, fructose, fucose, galactose, galacturonic acid, glucose, glucuronic acid, guluronic acid, mannose, mannuronic acid, rhamnose, ribose, and xylose) were purchased from Sigma-Aldrich (St. Louis, MO, USA). Dulbecco's modified eagle's medium (DMEM) was purchased from Solarbio (Beijing, China). Fetal bovine serum (FBS) and Trypsin were purchased from Gibco (Grand Island, NY, USA). Cell Counting Kit-8 (CCK-8) was purchased from Nuoyang Biotechnology Co., Ltd. (Hangzhou, China). Griess reagent was purchased from Beyotime Biotechnology Co., Ltd. (Shanghai, China). TRIzol was purchased from Invitrogen (Carlsbad, CA, USA). PrimeScript™ RT Master Mix and SYBR Green™ Premix Ex Taq™ II were purchased from Takara (Kyoto, Japan). The Mouse TNF-α ELISA kit and IL-6 ELISA kit were purchased from Multi Sciences Co., Ltd. (Hangzhou, China).

The RAW 264.7 cells were obtained from the Type Culture Collection of the Chinese Academy of Sciences (Shanghai, China).

Preparation of MBPs

Mulberry branch (Jialing20) was harvested and preprocessed according to the previous literature [5]. Dried branch material was crushed, decolorized with methanol, baked to remove residual methanol at 50 ℃, and dissolved in deionized water (m:v = 1:10, 2 h each for 3 times) at 90 ℃. The supernatant was collected and concentrated under reduced pressure using the rotary evaporator (Rotavapor R-100, Büchi, Flawil, Switzerland) at 60 ℃. Anhydrous alcohol was added until 90% concentration, followed by precipitation overnight to obtain crude polysaccharides. Protein impurities in the crude polysaccharides were removed using the Sevag method [19]. Briefly, the crude sample, chloroform, and n-butanol were fully mixed at a volume ratio of 25:4:1 and centrifuged at 8000 r/min for 10 min. After repeating several times with the supernatant until there was no noticeable precipitation between two phases, the sample was concentrated under reduced pressure using the rotary evaporator. Experimental MBPs were obtained by freeze drying to constant weight with the freeze dryer (Lab-1C-50E, Biocool, Beijing, China).

The MBPs (3 g) were dissolved in deionized water to a final concentration of 30 mg/mL and then loaded onto a cellulose DEAE-52 column (55 × 150 mm). Elution was performed with graded NaCl (0, 0.1, 0.2, 0.5, 1, and 2 mol/L), and the eluate per 10 mL was collected by tubes and detected by the phenol–sulfuric acid method [20]. Corresponding elution curve was generated.

The main DEAE-elution fraction was processed for dialysis, followed by further purification with the Sephadex G-100 column (16 × 800 mm). Elution was performed using deionized water, and the eluate per 10 mL was collected by tubes and detected by the phenol–sulfuric acid method. The equivalent fractions were pooled and marked as MBP-2.

Molecular weight determination

The average molecular weight of MBP-2 was analyzed by HPGPC [21] on an Waters 1515 instrument (Waters, USA) equipped with an Waters 2414 Refractive Index using a Waters Ultrahydrogel 500 column (7.8 × 300 mm, 10 μm). The mobile phase was 0.1 mol/L sodium nitrate ($NaNO_3$) -deionized water solution. Isocratic elution was obtained at 1 mL/min flow rate. Calibration curve was drawn by using various standard polyethylene glycol (PEG), and the following equation was finally estimated: $\mathrm{Log(Mw)} = -0.5603\mathrm{T} + 12.973$, $R^2 = 0.9993$.

Monosaccharide composition analysis

Monosaccharide compositions were obtained by the high-performance anion-exchange chromatography (HPAEC) [22]. MBP-2 (5 mg) were dissolved in 2 mL 3 mol/L trifluoroacetic acid (TFA), hydrolyzed at 120 ℃ for 2 h, blow-dried with nitrogen flow, washed with methanol, and dried. Methanol washing was performed three times to remove TFA, and then the sample was dissolved in deionized water. The content (%) of each monosaccharide was determined using monosaccharide standard curves (13 monosaccharide standards).

The chromatography system was ICS-5000 (Thermofisher Scientific, USA) equipped with Dionex™ CarboPac™ PA20 chromatographic column (3 × 150 mm, 10 μm) (column temperature, 30 ℃; injection volume, 5 μL; flow rate, 0.5 mL/min). Gradient elution was performed using the mobile phase A (0.1 mol/L NaOH) and B (0.1 mol/L NaOH, 0.2 mol/L NaAc) and monitored with an electrochemical detector. The elution procedures were as below: 0–30 min, 5–20% B; 30–30.1 min, 20–40%

B; 30.1–45 min, 40% B; 45–45.1 min, 40–2.5% B; 45.1–60 min, 5% B.

Fourier-transform infrared (FT-IR) spectroscopy

Samples were analyzed with the Nicolet iZ-10 FT-IR spectrometer (Thermofisher Scientific, USA) in the spectral range (4000–500) cm^{-1} using pressed KBr tablets [23].

Glycosidic linkage analysis

Methylation reaction

MBP-2 (1.1 mg) were dissolved in 500 μL anhydrous dimethyl sulfoxide (DMSO) and then successively incubated with 1 mg NaOH (30 min) and 50 μL iodomethane (1 h). Subsequently, 1 mL deionized water and 2 mL CH_2Cl_2 were added to the solution and vortexed to mix. Centrifugation was performed to discard the upper aqueous phase. The procedure was repeated three times. The lower fraction (CH_2Cl_2) was evaporated to dryness, added with 100 μL 2 mol/L TFA at 120 ℃ for 90 min, and evaporated to dryness again. Then, 50 μL 2 mol/L aqueous ammonia and 50 μL 1 mol/L $NaBD_4$ were added to mix and placed at room temperature for 2.5 h. The reaction was terminated by addition of 20 μL glacial acetic acid, and the solution was then blow-dried with nitrogen flow. CH_3OH (250 μL) washing was performed twice, followed by blow-dryness with nitrogen flow again. 250 μL acetic anhydride was added, vortexed to mix, and reacted at 100 ℃ for 2.5 h. Deionized water (1 mL, 10 min) and CH_2Cl_2 (500 μL) were successively added and vortexed to mix. The lower CH_2Cl_2 phase was collected and processed for gas chromatography-mass spectrometry (GC–MS).

GC–MS

GC was performed using the Agilent 7890A GC system (Agilent Technologies, USA) with BPX70 chromatographic column (0.25 mm × 30 m × 0.25 μm, SGE, Australia), the parameters as follows: injection volume, 1 μL; splitting ratio, 10:1; high purity helium carrier gas; flow rate, 1 mL/min. The injection temperature was 260 ℃. The column temperature started from 140 ℃ (2 min) to 230 ℃ (3 min) at a rate of 3 ℃/min.

MS was performed using the Agilent 5977B Quadrupole MS-Detection System (Agilent Technologies, USA) with the following parameters: electron bombardment ion source (EI); injection temperature, 230 ℃; quadrupole temperature, 150 ℃; mass scan range (m/z): 30–600.

Nuclear magnetic resonance (NMR) analysis

Purified MBP-2 (30 mg) were dissolved in 0.5 mL deuterated water (D_2O) and centrifuged. The supernatant was collected and lyophilized. After repeating this cycle three times, the lyophilized sample was dissolved in 0.5 mL D_2O and then loaded on the Avance 500 MHz NMR spectrometer (Bruker, Germany) to determine the one- dimensional (^{1}H-NMR, ^{13}C-NMR) and two-dimensional (^{1}H-^{1}H COSY, NOESY, HSQC, HMBC) NMR spectra[24].

Cell viability analysis

Cell culture

RAW 264.7 cells were cultured in complete Dulbecco's modified Eagle medium (DMEM) (supplemented with 10% FBS and 1% penicillin–streptomycin) in an incubator with a temperature of 37 ℃ and 5% CO_2.

CCK-8 assay

RAW 264.7 cells were inoculated into a 96-well plate at 5×10^4 cells/well and cultured overnight in a 37 ℃ incubator with 5% CO_2. Subsequently, MBP-2 at different concentrations (1, 10, 50, 100, 200, 400, and 800 μg/mL) were added. 1 μg/mL LPS was added as positive control, while MBP-free medium of equal volume was added as blank control. After 24 h of incubation, CCK-8 method was performed with the optical density at a certain wavelength calculated. Cell survival rate was correspondingly obtained.

NO assay

RAW 264.7 cells were cultured in mediums containing MBP-2 at different concentrations (50, 100, 200, and 400 μg/mL). The supernatant was collected after 24 h, and NO level was determined at 540 nm using an assay kit (Beyotime Biotechnology, Shanghai, China). 1 μg/mL LPS was added as positive control, while MBP-free medium of equal volume was added as blank control.

RT-qPCR

RAW 264.7 cells were inoculated into a 12-well plate (1×10^6 cells/well) and cultured overnight in an incubator with 5% CO_2 and a temperature of 37 ℃. MBPs at different concentrations (50, 100, 200, and 400 μg/mL) were added to the cells. 1 μg/mL LPS was added as positive control, while MBP-free medium of equal volume was added as blank control. Each group contained 3 replicates. After 24 h, total RNA was extracted using Trizol according to the instructions and reversely transcribed into cDNA with the PrimeScript™ RT Master Mix (Takara, Kyoto, Japan). The cDNA was amplified by the PCR kit (TaKaRa), and RT-qPCR was performed using the Mastercycler (Eppendorf, Hamburg, Germany). GAPDH was used as the internal reference. Primer information was detailed in Table 1.

Table 1 Primer sequences conditions for RT-qPCR primers

Gene	Forward	Reverse
iNOS	GTTCTCAGCCCAACAATACAAGA	GTGGACGGGTCGATGTCAC
IL-1β	GGTGTGTGACGTTCCCATTA	ATTGAGGTGGAGAGCTTTCAG
IL-6	TAGTCCTTCCTACCCCAATTTCC	CGCACTAGGTTTGCCGAGTA
MCP-1	TCGCTCTGCTTGCTGCCATTC	ACGTCCTGATCCTCTGCCTGTG
GAPDH	AACAGGGTGGTGGACCTCAT	GGGATAGGGCCTCTCTTGCT

Examination of cytokine (IL-6, TNF-α)

RAW 264.7 cells were inoculated into a 12-well plate at 1×10^6 cells/well and cultured overnight in a 37 ℃ incubator with 5% CO_2. Subsequently, MBP-2 at different concentrations (1, 10, 50, 100, 200, and 400 μg/mL) were added. 1 μg/mL LPS was added as positive control, while MBP-free medium of equal volume was added as blank control. Each group contained 3 replicates. After 24 h, the cell suspension was centrifuged at 1000×*g* for 10 min. The supernatant was collected and processed for determination of IL-6 and TNF-α levels using the ELISA kit (Multi Sciences).

The effect of MBP-2 on the production of IL-6 and TNF-α by RAW 264.7 cells was explored using TAK-242 (TLR4 inhibitor) and C29 (TLR2 inhibitor). Cell culture and cytokine examination were performed with the following grouping strategy: Blank control (Ctrl group), TAK-242 inhibitor group (TAK group), C29 inhibitor group (C29 group), MBPs group (MBP-2 group), and inhibitor + MBPs group (TAK + MBP-2, C29 + MBP-2, and TAK + C29 + MBP-2 group). Concentration of each reagent was 10 μg/mL for MBP-2, 1 μM for TAK-242, and 50 μM for C29. MBPs were added 1 h after addition of inhibitors. Each group contained 3 replicates.

Statistical analysis

One-way analysis of variance (ANOVA) with multiple comparisons (Bonferroni's correction) (> 2 group studies) was applied to identify differences among groups (GraphPad Pro Prism 8.0). *P* value less than 0.05 was considered statistically significant.

Results and discussions

Purification, molecular weight, monosaccharide composition, and FT-IR spectrum of MBP-2

As shown in Fig. 1A, the main DEAE-elution fraction comprised the majority of crude MBPs, marked as MBP-1. The MBP-1 was dialyzed using a 3 kDa dialysis bag, and the glucan gel-purified sample was labelled as MBP-2 (Additional file 1: Fig. S1).

As analyzed by HPGPC (Fig. 1B), a single symmetric peak occurred at around 21.5 min, suggesting favorable homogeneity of the MBP-2. Further molecular weight fitting analysis demonstrated its number averaged molecular weights (Mn) as 15.3 kDa and weight-averaged molecular weights (Mw) as 21.7 kDa, and the Mw was smaller than the previous report [10, 25].

The ion chromatogram of monosaccharide composition of the MBP-2 was shown in Fig. 1C. Glucose was the main monosaccharide, indicating the potential glucan structure of the MBP-2. There was a distinct difference from the previous report in terms of the monosaccharide composition of MBPs [10, 25].

As displayed in FT-IR in Fig. 1D, a broad and intense absorption peak for stretching vibration of O–H appeared at 3431 cm^{-1}, while an absorption peak for stretching vibration of C–H as the characteristic peak of saccharides appeared at 2926 cm^{-1}[26]. The absorption peak at 1634 cm^{-1} was attributed to the stretching vibration of C–O [27]. The appearance of an absorption peak at 931 cm^{-1} demonstrated asymmetric stretching vibration of the pyranose ring of D-glucose [28]. Besides, the stretch peak was at 849 cm^{-1}, demonstrating α-glycosidic linkage [29]. Thus, the MBP-2 might be composed of D-glucose and α-glycosidic linkages [30]. No distinct peak were noticed at 1730 cm^{-1} and 1240 cm^{-1}, which implied the absence of uronic acid [31, 32], consistent with the monosaccharide composition analysis.

Methylation analysis

GC–MS was performed following methylation reactions, and the total ion chromatogram was shown in Additional file 1: Fig. S2. Peak analysis demonstrated that, there were three main peaks (peak 1, 2, and 3) with the retention time of 8.87, 14.12, and 18.27 min, and the relative molar amount of 11.4%, 78.5%, and 6.75%, respectively (Table 2). The primary fragments pointed out that the MBP-2 sample was mainly composed of a backbone linked by →4)-*α*-D-Glc*p*-(1→ and contains *α*-D-Glc*p*-(1→ and →4, 6)-*α*-D-Glc*p*-(1→ (Additional file 1: Fig. S3).

NMR analysis

NMR was performed to further characterize the structure of saccharide subunits of MBP-2. The major hydrogen signals of MBP-2 varied between δ 3 and 5.5 ppm in ^{1}H-NMR (Fig. 2A) while between δ 60 and 105 ppm in ^{13}C-NMR (Fig. 2B). Usually, most of the α-anomeric protons vary between 5–6 ppm and the β-anomeric protons vary between 4–5 ppm [33]. Here, an anomeric proton signal appeared at δ 5.3 ppm in ^{1}H-NMR, demonstrating an α-configuration. In the meantime, an anomeric carbon signal appeared at δ 99.6 ppm in ^{13}C-NMR.

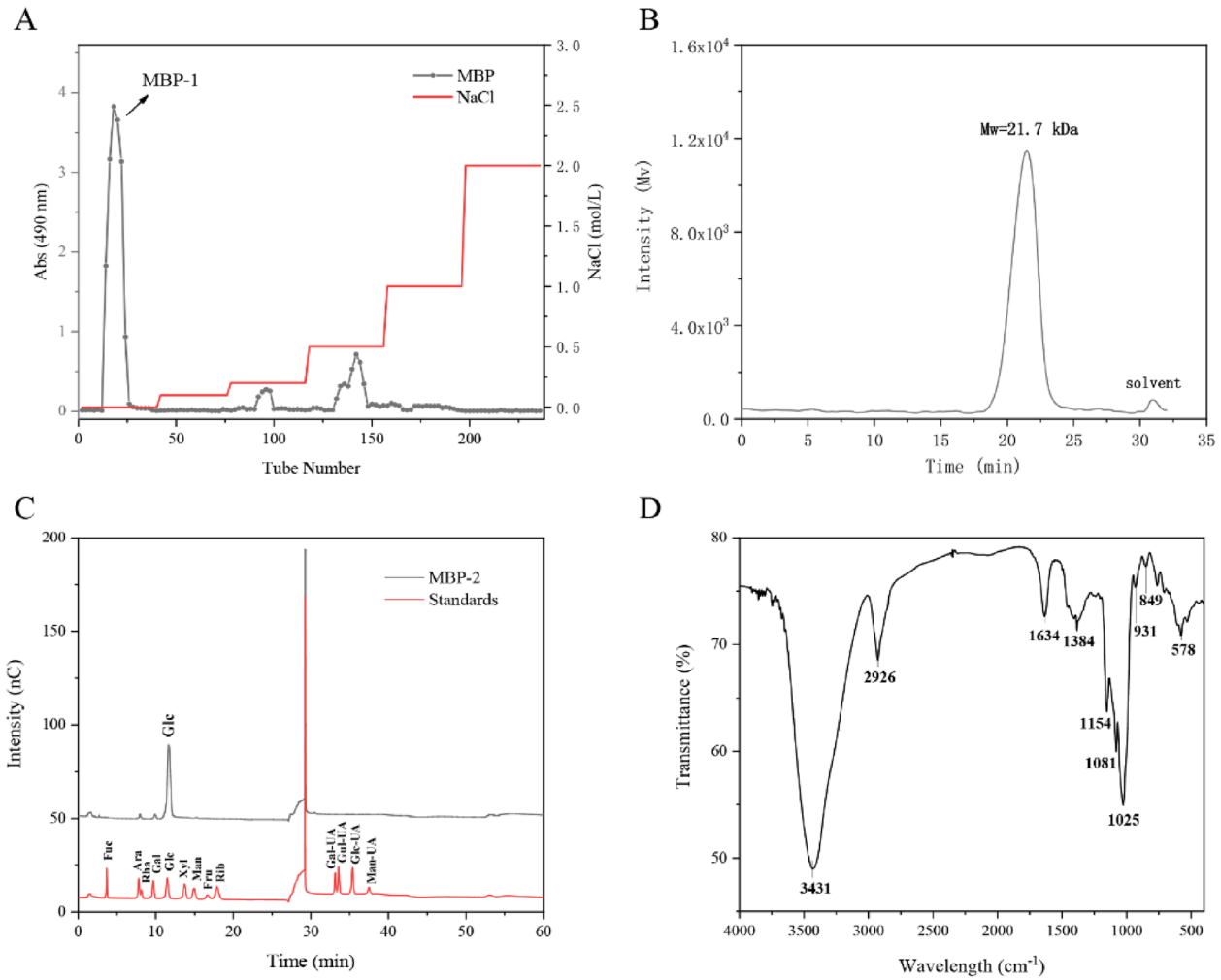

Fig. 1 Elution profile on DEAE-52 column (**A**). HPGPC spectrum of MBP-2 (**B**). Ion chromatography profile of MBP-2 (**C**). FT-IR spectrum of MBP-2 (**D**)

Table 2 Methylation analysis for MBP-2

Time (min)	Major mass fragments (*m/z*)	Deduced residues	Molar ratio
8.87	239.19, 205.11, 162.08, 145.08, 118.05, 102.06, 87.04	T-Glc(p)	1
14.12	233.09, 162.07, 118.06, 87.05	4-Glc(p)	6.88
18.27	261.09, 231.07, 201.06, 142.05, 118.05, 102.06, 59.04	4, 6-Glc(p)	0.59

Both signals were attributed to the H1 and C1 signals of →4)-*α*-D-Glc*p*-(1→ [34]. According to the relative intensity, the residues were labelled as A, B, and C from high to low. The results of GC–MS showed that residue A had the highest intensity as 78.5%. Correspondingly, residue A had the strongest signals in ^{1}H-NMR and ^{13}C-NMR, and the signals at δ 3.9, 3.78, 3.77, 3.58 ppm, except δ 5.34 ppm, all could be attributed to the hydrogen signals of residue A. Similarly, the signals at δ 99.6, 76.8, 73.3, 71.6, 71.2, and 60.5 ppm in ^{13}C-NMR were carbon signals of residue A. Based on the cross-peak signals in ^{1}H-^{1}H COSY, the hydrogen signals of residue A, including H1, H2, H3, H4, and H5, were δ 5.34, 3.55, 3.91, 3.61, and 3.77 ppm, respectively (Fig. 2C). While based on the cross-peak signals in HSQC, the carbon signals C1, C2, C3, C4, and C5 were, respectively δ 99.56, 71.58, 73.29, 76.81, and 71.24 ppm (Fig. 2F). The chemical shifts of H6a/6b (δ 3.79, and 3.54 ppm) and C6 (δ 60.51 ppm)

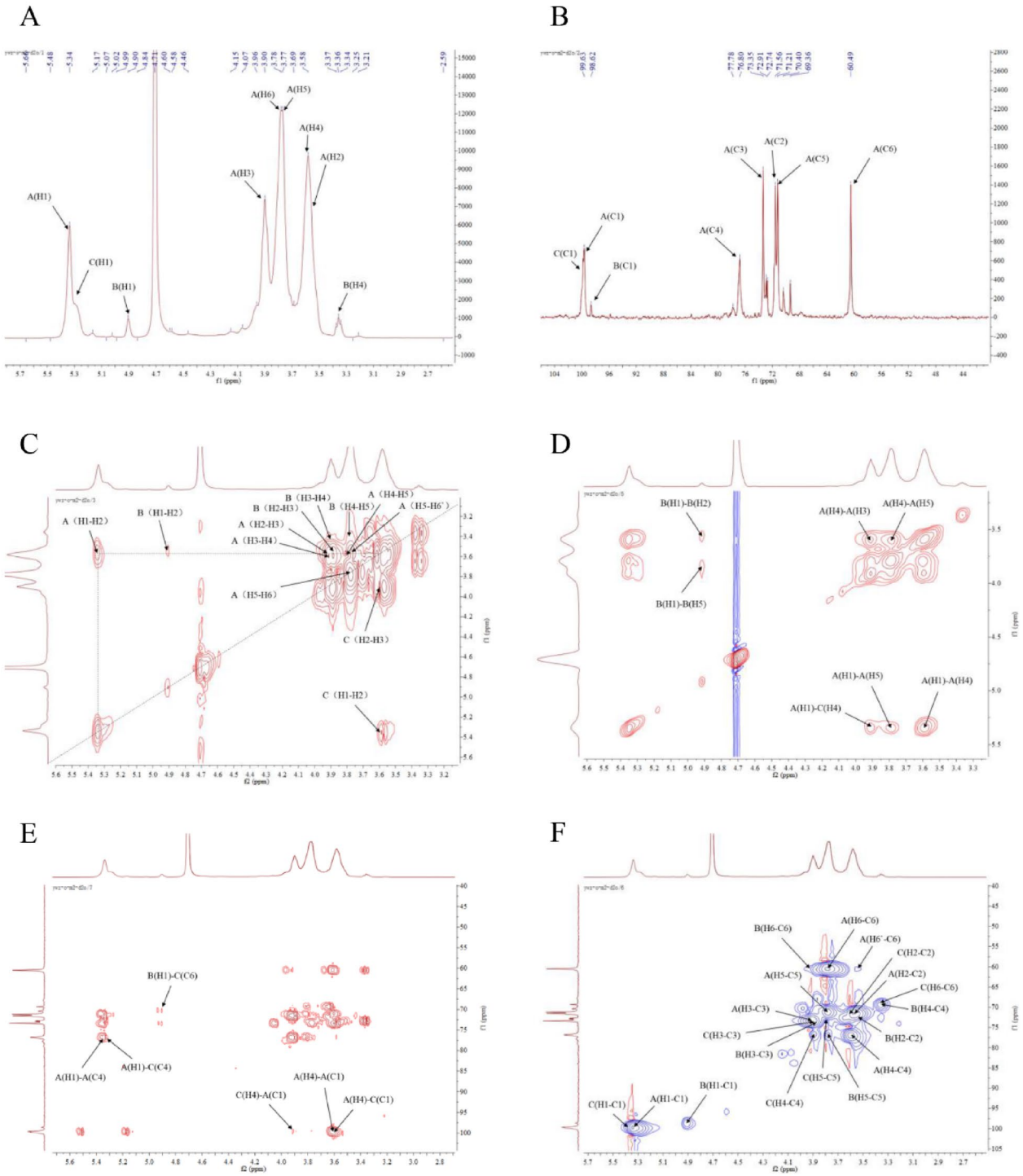

Fig. 2 ^{1}H-NMR (**A**), ^{13}C-NMR (**B**), ^{1}H-^{1}H COSY (**C**), NOESY (**D**), HMBC (**E**) and HSQC (**F**) spectrum of MBP-2

were also obtained from HSQC. The downfield shift of C4 also indicated that the residue A was →4)-*α*-D-Glc*p*-(1→. The above results were also supported by previous reports [35, 36].

As for residue B, the signals of H1, H2, H3, H4 and H5 were obtained from the ^{1}H-^{1}H COSY (Fig. 2C), which was δ 4.91, 3.54, 3.88, 3.36, and 3.77 ppm, respectively. The chemical shifts of H6a/6b were supported by HSQC

spectrum (Fig. 2F). All the 13C chemical shifts of residue B were also obtained from HSQC. Relative to A–C4, B–C4 did not develop downfield shift given the absence of substituents at the C4 site, consistent with the previous literature [37]. The chemical shift of residue C signals and corresponding attributes were obtained using the same method and shown in Table 3.

HMBC spectrum can display the inter-residue connectivities with glycosidic bonds. As shown in Fig. 2E, there were cross-peaks between A–H4 (3.36 ppm) and A–C1 (99.56 ppm), and between A–H1 (5.34 ppm) and A–C4 (76.81 ppm), demonstrating a → 4)-*α*-D-Glc*p*-(1 → 4)-*α*-D-Glc*p*-(1 → (i.e., 4A1 → 4A1) structure. The cross-peaks between A–H1 (5.34 ppm) and C–C4 (76.72 ppm) and between C–H4 (3.90 ppm) and A–C1 (99.56 ppm) indicated a → 4)-*α*-D-Glc*p*-(1 → 4, 6)-*α*-D-Glc*p*-(1 → 4)-*α*-D-Glc*p*-(1 → (i.e., 4A1 → 4, 6C1) structure. The cross-peaks between A–H4 (3.61 ppm) and C–C1 (99.94 ppm) implied a → 4, 6)-*α*-D-Glc*p*-(1 → 4)-*α*-D-Glc*p*-(1 → (i.e., 4A1 → 4, 6C1) structure. The cross-signals between B-H1 (4.91 ppm) and C–C6 (69.32 ppm) suggested a *α*-D-Glc*p*-(1 → 6, 4)-*α*-D-Glc*p*-(1 → (i.e., B1 → 6, 4C1) structure.

In the NOESY spectrum (Fig. 2D), the cross-peaks between A (H1) and A (H4), except for the existing signals in ^{1}H-^{1}H COSY, further demonstrated the presence of the 4A1 → 4A1 structure, while the cross-peaks between A (H1) and C (H4) indicated the 4A1 → 4, 6C1 structure. Additionally, the glucose at positions 1 and 5 formed a ring, resulting in cross-peaks between A (H1) and A (H5) and between B (H1) and B (H5). The results were in line with the results of HMBC. Combining the above findings, the structure of MBP-2 might be characterized as that in Fig. 3.

Currently, glucan polysaccharides have been only reported in the root of white mulberry, while they are starchy polysaccharides with low water solubility [38]. The present study, for the first time, identified glucan polysaccharides from mulberry branch, which are water-soluble and worthy of further development and utilization.

Immunoregulatory activity

Cell survival and NO content

To assess the safety of MBP-2, CCK-8 was performed to detect the viability of RAW 264.7 cells treated with MBP-2 (1–800 μg/mL) (Fig. 4A). The result demonstrated that MBP-2 at a low concentration (1–10 μg/mL) significantly promoted the proliferation in RAW 264.7 cells ($P < 0.05$). Besides, the cell proliferation decreased when the concentration of MBP-2 increased, and the decline was extremely significant upon 800 μg/mL ($P < 0.01$). Thus MBP-2 at 400 μg/mL was selected as the highest concentration in further analysis.

NO is an important molecular messenger that can mediate a series of host-defense functions executed by activated macrophages. In addition, it is also a type of

Table 3 1H and 13C NMR chemical shifts of MBP-2 recorded in D_2O

	Glycosyl residues	H1/C1	H2/C2	H3/C3	H4/C4	H5/C5	H6a,b/C6	
A	→ 4)-*α*-D-Glc*p*-(1 →	5.34	3.55	3.91	3.61	3.77	3.79	3.54
		99.56	71.58	73.29	76.81	71.24	60.51	
B	*α*-D-Glc*p*-(1 →	4.91	3.54	3.88	3.36	3.77	3.89	3.37
		98.58	71.7	73.29	69.32	76.71	60.51	
C	→ 4,6)-*α*-D-Glc*p*-(1 →	5.34	3.59	3.89	3.90	3.78	3.38	
		99.94	71.66	73.33	76.72	71.27	69.32	

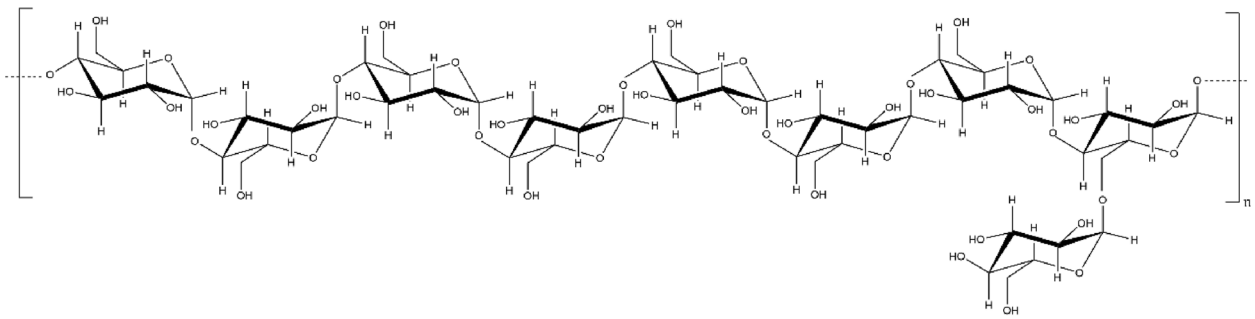

Fig. 3 Chemical structural of MBP-2

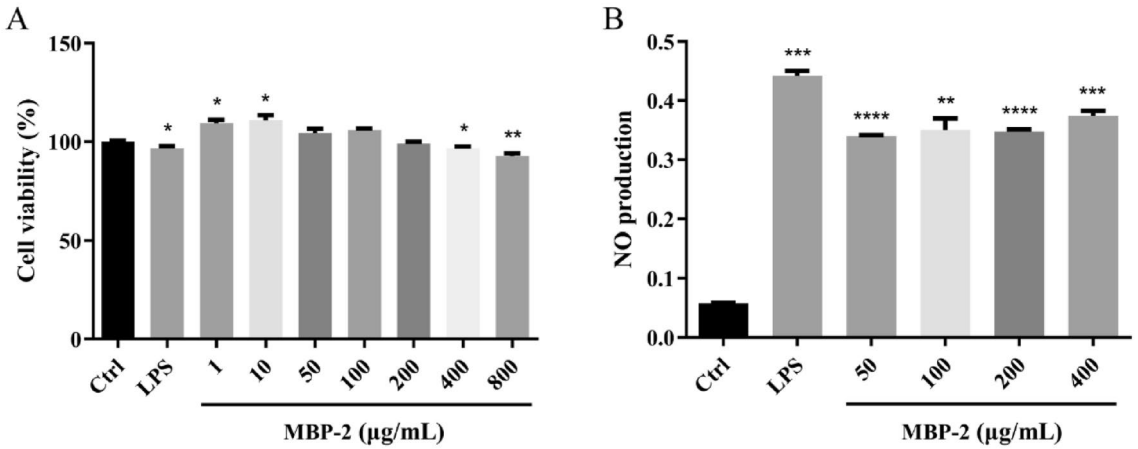

Fig. 4 Effect of MBP-2 on cell viability (**A**) and NO production (**B**) of RAW 264.7 cells. $^{*}P < 0.05$, $^{**}P < 0.01$, and $^{***}P < 0.001$ compared to Ctrl

cytotoxic agent with immunoregulatory activity [39]. To explore the potential immunoregulatory activity of MBP-2, the NO produced by RAW 264.7 cells was examined. As shown in Fig. 4B, MBP-2 at 50–400 μg/mL remarkably activated the production of NO by RAW 264.7 cells, consistent with the positive control (LPS). This suggested that MBP-2 might have immunostimulatory effects.

Expression of relevant cellular genes

Inducible nitric oxide synthase (iNOS) can act through NO synthesis [40]. The immunoregulatory activity of native products is largely attributed to their capability of inducing multiple chemokines (e.g., MCP-1) and cytokines (e.g., TNF-α, IL-6) [41, 42]. This study analyzed the effect of MBP-2 on expression of relevant genes in RAW 264.7. It was found that MBP-2 at 50–400 μg/mL significantly stimulated the expression of iNOS in RAW 264.7 cells (Fig. 5A), consistent with the positive control (LPS) and NO production trend (Fig. 4B). The result indicated that MBP-2 could activate the cellular defense functions by up-regulating iNOS expression and inducing NO synthesis. Moreover, MBP-2 also led to distinct up-regulation of IL-1β, IL-6, and MCP-1 gene in RAW 264.7 cells (Fig. 5B–D), thereby exerting its immunoregulatory activity.

Cytokine level

Cytokine is a class of bioactive macromolecular proteins that are produced upon an external stimulus to immune cells and play an important role in regulating the body's immunity and inflammatory response [43, 44]. Pro-inflammatory cytokines TNF-α and IL-1β can act on macrophages to enhance immune responses and induce the expression of other immunoregulatory factors [45]. The current study found that MBP-2 significantly elevated the expression of TNF-α and IL-6 (Fig. 6A, B), thereby exerting its immunoregulatory activity.

The above findings demonstrated favorable immunoregulatory activity of MBP-2. It was reported that the immunoregulatory activity of MBPs might be attributed to their (1→4)-α-D-glucan backbone [46]. The immunoregulatory polysaccharides from traditional Chinese medicines have been applied in development of vaccines as adjuvants to promote the immune response of the body [47, 48]. Therefore, the MBP-2 may have the potential to be used as vaccine adjuvants.

The secretion of cytokines (IL-1β and TNF-α) can be mediated by multiple signals, among which Toll-like receptor (TLR) is the most significant [49]. Native polysaccharides can modulate immune cell functions in vitro by interactions with immunoreceptors, such as TLRs [50]. To investigate the mechanism underlying the immunoregulatory activity of MBP-2, this study selected C29 and TAK-242 for analysis. C29 is a TLR2 inhibitor that can block hTLR2/1 and hTLR2/6 signals [51]. TAK-242, also known as Resatorvid, is a selective inhibitor of TLR4 signal transduction that can down-regulate the expression of TLR4 downstream signaling molecule Myeloid differentiation factor 88 (MyD88) and TIR-domain-containing adaptor inducing interferon-β (TRIF) [52, 53]. As analyzed, TAK-242 dramatically suppressed the production of IL-6 ($P < 0.01$), and the IL-6 level was not significantly different with that of the Ctrl group (Fig. 6C). The result suggested that TAK-242 can inhibit the immunoregulatory activity of MBP-2. In addition, IL-6 production was also decreased by C29, but the effect was largely different with that of the Ctrl and TAK groups ($P < 0.01$). Similar results were obtained for TNF-α (Fig. 6D). However, there was a large difference between the Ctrl and

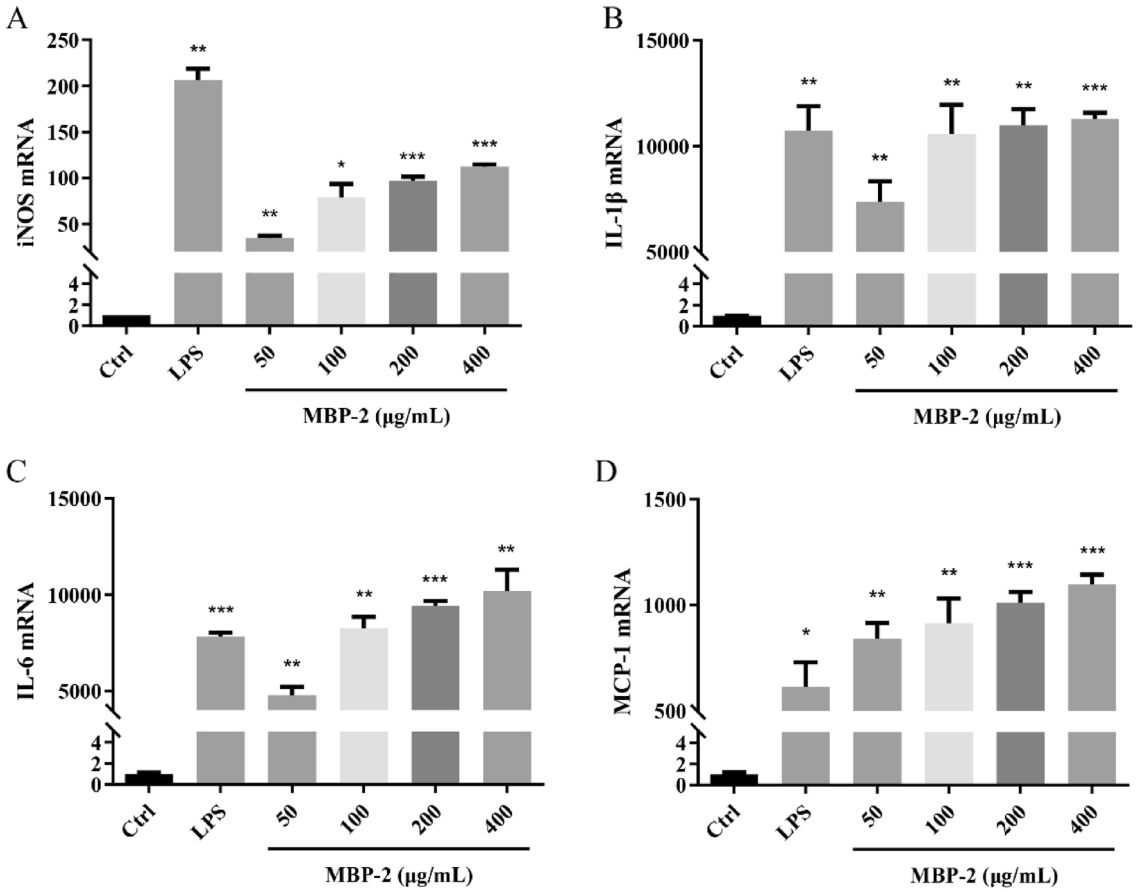

Fig. 5 mRNA levels of iNOS (**A**), IL-1β (**B**), IL-6 (**C**) and MCP-1 (**D**) as determined by RT-qPCR. $^{*}P<0.05$, $^{**}P<0.01$, and $^{***}P<0.001$ compared to Ctrl

TAK groups when the MBP-2 concentration was too high or the concentration of inhibitors was too low, which might be due to the large stimulating effect of 10 μg/mL MBP-2 on TNF-α production. In general, the trend for IL-6 and TNF-α production was similar, and the TAK-242 was more potent than C29 in inhibiting their production ($P<0.01$). Collectively, MBP-2 may exert its immunoregulatory activity via TLR4, during which TLR2-related pathways are potential participants.

Research has revealed that TLR2 regulates downstream mitogen-activated protein kinase (MAPK) and nuclear factor kappa-B (NF-κB) via MYD88-dependent pathways, thereby playing its immune-stimulating effect. Except the MYD88-dependent pathways, TLR4 can also play its role through the TRIF pathway [54]. The current study found that the TLR4 inhibitor, TAK-242, had more significant suppressive effect on cytokine production in cells treated with MBP-2, as compared to the TLR2 inhibitor C29, indicating that MBP-2 acted mainly via the TRIF-dependent pathways while the MYD88 pathways might also make some contributions. Since the immunoregulatory activity of MBPs has been rarely reported, further studies are required.

Conclusion

The present study obtained the main neutral sugar, named MBP-2, from mulberry branch through Sephadex G-100 gel purification. Their molecular weight is around 21.7 kDa, and they are mainly composed of a backbone linked by →4)-*α*-D-Glc*p*-(1→ and contains *α*-D-Glc*p*-(1→ and →4, 6)-*α*-D-Glc*p*-(1→. MBP-2 can significantly enhance the NO release from RAW 264.7 cells and exert their immunoregulatory activity via increasing the mRNA expression of relevant inflammatory factors (IL-6 and TNF-α) and promoting their release. With reference to the mechanism, we speculated that MBP-2 exert the immunoregulatory activity mainly via the downstream TRIF-dependent signaling pathways activated by TLR4 receptors. This study, for the first time, reported the glucan polysaccharides from mulberry branch and their immunoregulatory activity, providing new insight into the pharmacological

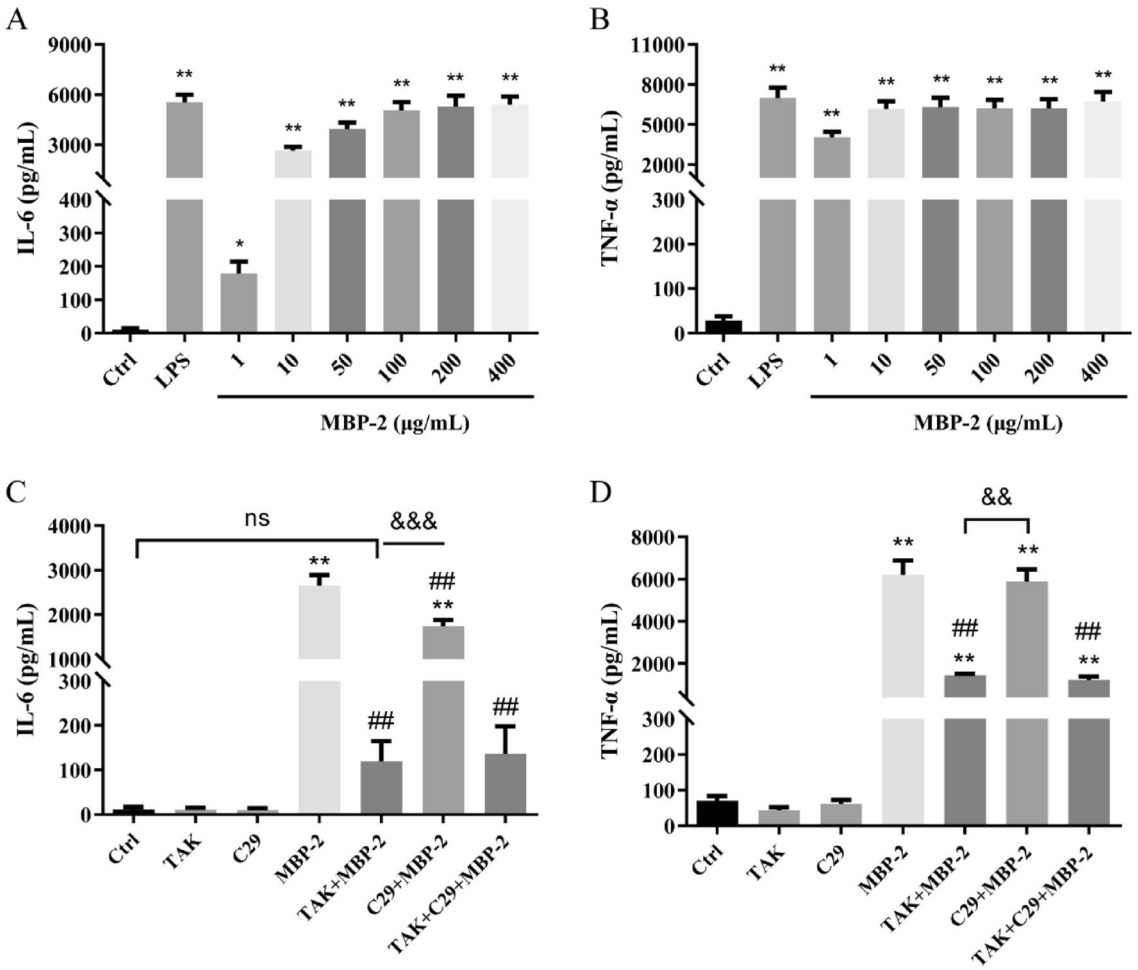

Fig. 6 Expression of cytokines in RAW 264.7 **A**–**D**: **A** effect of MBP-2 on the expression of IL-6; **B** effect of MBP-2 on the expression of TNF-α; **C** effect of TLRs inhibitors on the expression of IL-6; **D** effect of TLRs inhibitors on the expression of TNF-α. $^{*}P < 0.05$, $^{**}P < 0.01$, and $^{***}P < 0.001$ compared to Ctrl; $^{\#\#}P < 0.01$ compared to MBP-2; $^{\&\&}P < 0.01$, and. $^{\&\&\&}P < 0.001$ compared to TAK + MBP-2

activity of mulberry branch and its development and utilization.

Supplementary Information

The online version contains supplementary material available at https://doi.org/10.1186/s40538-024-00563-3.

Additional file 1: Figure. S1. Elution curve of MBP-2 on Sephadex G-100. **Fig. S2.** GC-MS total ion chromatogram of MBP-2. **Fig. S3.** Fragments mass spectrum of peak 1 (**A**), 2 (**B**) and 3 (**C**) in GC-MS.

Acknowledgements
Not applicable.

Author contributions
Wei Xiang: conceptualization, methodology, formal analysis, investigation, data curation, writing–review and editing, funding acquisition. Li Xu: resources, supervision. Li Zheng: validation, data curation. Qi-ao Zhang: data curation. Xiaowen Shi: visualization, project administration, funding acquisition. All authors read and approved the manuscript.

Funding
This work was supported by the grants from Zhejiang Provincial Health Bureau Science Foundation, Hangzhou, China (No. 2022KY1253 to X.S.), and China Postdoctoral Science Foundation funded project (No. 2023MD744147 to W. X.).

Availability of data and materials
Not applicable.

Declarations

Ethics approval and consent to participate
Not applicable.

Consent for publication
Not applicable.

Competing interests
The authors declare that they have no competing interests.

Author details
[1]Chongqing College of Traditional Chinese Medicine, Chongqing 402760, China. [2]Chongqing Institute of Traditional Chinese Medicine, Chongqing Traditional Chinese Medicine Hospital, Chongqing 400011, China. [3]State Key Laboratory of Silkworm Genome Biology, Key Laboratory of Sericultural Biology and Genetic Breeding, College of Sericulture, Textile and Biomass Sciences, Ministry of Agriculture and Rural Affairs, Southwest University, Chongqing 400715, China. [4]The Second Affiliated Hospital of Jiaxing University, Jiaxing 314000, Zhejiang, China.

Received: 20 January 2024 Accepted: 5 March 2024
Published online: 13 March 2024

References

1. Yang S, Wang BL, Xia XJ, Li X, Wang RY, Sheng L, et al. Simultaneous quantification of three active alkaloids from a traditional Chinese medicine Ramulus Mori (Sangzhi) in rat plasma using liquid chromatography-tandem mass spectrometry. J Pharm Biomed Anal. 2015;109:177–83. https://doi.org/10.1016/j.jpba.2015.02.019.
2. Yu WS, Chen H, Xiang ZH, He NJ. Preparation of polysaccharides from Ramulus mori, and their antioxidant, anti-inflammatory and antibacterial activities. Molecules. 2019;24(5):24050856. https://doi.org/10.3390/molecules24050856.
3. Feng Z, Peng S, Wu ZY, Jiao LA, Xu SW, Wu Y, et al. Ramulus mori polysaccharide-loaded PLGA nanoparticles and their anti-inflammatory effects in vivo. Int J Biol Macromol. 2021;182:2024–36. https://doi.org/10.1016/j.ijbiomac.2021.05.200.
4. Lu HP, Jia YN, Yu Y, Xu L. DNA protection activity of a hydroethanol extract and six polyphenol monomers from *Morus alba* L. (mulberry) twig. Int J Food Prop. 2017;20(S2):2207–19. https://doi.org/10.1080/10942912.2017.1368554.
5. Xiang W, Xia ZN, Xu L. UPLC-MS/MS profiling, antioxidant, α-glucosidase inhibitory, cholinesterase inhibitory, and cardiovascular protection potentials of Jialing 20 (*Morus multicaulis* Perr.) Mulberry Branch Extract. Foods. 2021;10(11):2659. https://doi.org/10.3390/foods10112659.
6. Feng FS, Xiang W, Gao H, Jia YA, Zhang YS, Zeng LS, et al. Rapid screening of nonalkaloid alpha-glucosidase inhibitors from a Mulberry twig extract using enzyme-functionalized magnetic nanoparticles coupled with UPLC-MS/MS. J Agric Food Chem. 2022;70(38):11958–66. https://doi.org/10.1021/acs.jafc.2c03435.
7. Zhu YY, Xiang W, Shen Y, Jia YA, Zhang YS, Zeng LS, et al. New butyrylcholinesterase inhibitor derived from mulberry twigs, a kind of agricultural byproducts. Ind Crops Prod. 2022;187(B):115535. https://doi.org/10.1016/j.indcrop.2022.115535.
8. Ji XL, Guo JH, Tian JY, Ma K, Liu YQ. Research progress on degradation methods and product properties of plant polysaccharides. J Light Ind. 2023;38(3):55–62. https://doi.org/10.12187/2023.03.007.
9. Kakar MU, Kakar IU, Mehboob MZ, Zada S, Soomro H, Umair M, et al. A review on polysaccharides from *Artemisia sphaerocephala* Krasch seeds, their extraction, modification, structure, and applications. Carbohydr Polym. 2021;252:117113. https://doi.org/10.1016/j.carbpol.2020.117113.
10. He XR, Fang JC, Ruan YL, Wang XX, Sun Y, Wu N, et al. Structures, bioactivities and future prospective of polysaccharides from *Morus alba* (white mulberry): a review. Food Chem. 2018;245:899–910. https://doi.org/10.1016/j.foodchem.2017.11.084.
11. Chen RH, Zhou X, Deng QF, Yang MH, Li SY, Zhang QR, et al. Extraction, structural characterization and biological activities of polysaccharides from mulberry leaves: a review. Int J Biol Macromol. 2024;257:128669. https://doi.org/10.1016/j.ijbiomac.2023.128669.
12. Chen Y, Jiang X, Xie H, Li X, Shi L. Structural characterization and antitumor activity of a polysaccharide from Ramulus mori. Carbohydr Polym. 2018;190(15):232–9. https://doi.org/10.1016/j.carbpol.2018.02.036.
13. Qiu F, He TZ, Zhang YQ. The isolation and the characterization of two polysaccharides from the branch bark of mulberry (*Morus alba* L.). Arch Pharm Res. 2016;39(7):887–96. https://doi.org/10.1007/s12272-016-0742-8.
14. Li X, Wang L, Gao X, Li G, Cao H, Song D, et al. Mechanisms of protective effect of Ramulus mori polysaccharides on renal injury in High-Fat Diet/Streptozotocin-Induced Diabetic Rats. Cell Physiol Biochem. 2015;37(6):2125–34. https://doi.org/10.1159/000438570.
15. Yang Q, Cai XX, Huang MC, Wang SY. A specific peptide with immunomodulatory activity from *Pseudostellaria heterophylla* and the action mechanism. J Funct Foods. 2020;68:103887. https://doi.org/10.1016/j.jff.2020.103887.
16. Cui LN, Chen L, Yang G, Li YK, Qiao ZH, Liu Y, et al. Structural characterization and immunomodulatory activity of a heterogalactan from *Panax ginseng* flowers. Food Res Int. 2021;140:109859. https://doi.org/10.1016/j.foodres.2020.109859.
17. Yao Y, Zhu YY, Ren GX. Immunoregulatory activities of polysaccharides from mung bean. Carbohydr Polym. 2016;139:61–6. https://doi.org/10.1016/j.carbpol.2015.12.001.
18. Yin ZH, Liang ZH, Li CQ, Wang JM, Ma CY, Kang WY. Immunomodulatory effects of polysaccharides from edible fungus: a review. Food Sci Hum Well. 2021;10(4):393–400. https://doi.org/10.1016/j.fshw.2021.04.001.
19. Zhu HJ, Tian L, Zhang L, Bi JX, Song QQ, Yang H, et al. Preparation, characterization and antioxidant activity of polysaccharide from spent *Lentinus edodes* substrate. Int J Biol Macromol. 2018;112:976–84. https://doi.org/10.1016/j.ijbiomac.2018.01.196.
20. Dubois M, Gilles KA, Hamilton JK, Rebers PA, Smith F. Colorimetric method for determination of sugars and related substances. Anal Chem. 1956;28(3):350–6. https://doi.org/10.1021/ac60111a017.
21. Liu SS, Shi XW, Xiang W, Jin ZH, Jia YA, Zhang YS, et al. Bioactivities and physicochemical properties of crude polysaccharides from mulberry twigs, agricultural by-products. Ind Crops Prod. 2023;193:116191. https://doi.org/10.1016/j.indcrop.2022.116191.
22. Cui MX, Cheng L, Shen YF, Liu KH, Liu KW. Structural characterization, hypoglycemic and immune-enhancing activities of a polysaccharide from *Oenanthe javanica*. J Food Meas Charact. 2023;17:6318–29. https://doi.org/10.1007/s11694-023-02121-1.
23. Sun JR, Li JL, Yao LL, You FF, Yuan JF, Wang DH, et al. Synthesis, characterization and antioxidant activity of selenium nanoparticle decorated with polysaccharide from hawthorn. J Food Meas Charact. 2023;17:6125–34. https://doi.org/10.1007/s11694-023-02124-y.
24. Zhang ZF, Song TT, Lv GY, Liu J, Jin QL. Structural properties and immunomodulatory activity of an α-glucan purified from the fruiting body of *Stropharia rugosoannulata*. Chem Biol Technol Ag. 2023;10(1):100. https://doi.org/10.1186/s40538-023-00475-8.
25. Ai J, Bao B, Battino M, Giampieri F, Chen C, You LJ, et al. Recent advances on bioactive polysaccharides from mulberry. Food Funct. 2021;12(12):5219–35. https://doi.org/10.1039/d1fo00682g.
26. Zhan Q, Wang Q, Lin R, He P, Lai F, Zhang M, et al. Structural characterization and immunomodulatory activity of a novel acid polysaccharide isolated from the pulp of *Rosa laevigata* Michx fruit. Int J Biol Macromol. 2020;145:1080–90. https://doi.org/10.1016/j.ijbiomac.2019.09.201.
27. Tang N, Wang X, Yang R, Liu Z, Liu Y, Tian J, et al. Extraction, isolation, structural characterization and prebiotic activity of cell wall polysaccharide from *Kluyveromyces marxianus*. Carbohydr Polym. 2022;289:119457. https://doi.org/10.1016/j.carbpol.2022.119457.
28. Liu AJ, Yu J, Ji HY, Zhang HC, Zhang Y, Liu HP. Extraction of a novel cold-water-soluble polysaccharide from *Astragalus membranaceus* and its antitumor and immunological activities. Molecules. 2017;23(1):62. https://doi.org/10.3390/molecules23010062.
29. Molaei H, Jahanbin K. Structural features of a new water-soluble polysaccharide from the gum exudates of *Amygdalus scoparia* Spach (Zedo gum). Carbohydr Polym. 2018;182:98–105. https://doi.org/10.1016/j.carbpol.2017.10.099.
30. Ji HY, Yu J, Liu AJ. Structural characterization of a low molecular weight polysaccharide from *Grifola frondosa* and its antitumor activity in H22 tumor-bearing mice. J Funct Foods. 2019;61:103472. https://doi.org/10.1016/j.jff.2019.103472.
31. Zhang AQ, Deng JY, Yu SY, Zhang FM, Linhardt RJ, Sun PL. Purification and structural elucidation of a water-soluble polysaccharide from the fruiting bodies of the *Grifola frondosa*. Int J Biol Macromol. 2018;115:221–6. https://doi.org/10.1016/j.ijbiomac.2018.04.061.
32. Ji XL, Cheng YQ, Tian JY, Zhang SQ, Jing YS, Shi MM. Structural characterization of polysaccharide from jujube (*Ziziphus jujuba* Mill.) fruit. Chem Biol Technol Agric. 2021;8(1):54. https://doi.org/10.1186/s40538-021-00255-2.

33. Li JW, Ai LZ, Yang Q, Liu YF, Shan L. Isolation and structural characterization of a polysaccharide from fruits of *Ziziphus jujuba* cv. Junzao. Int J Biol Macromol. 2013;55:83–7. https://doi.org/10.1016/j.ijbiomac.2012.12.017.
34. Chen H, Sun J, Liu J, Gou YR, Zhang X, Wu XN, et al. Structural characterization and anti-inflammatory activity of alkali-soluble polysaccharides from purple sweet potato. Int J Biol Macromol. 2019;131:484–94. https://doi.org/10.1016/j.ijbiomac.2019.03.126.
35. Wang JQ, Nie SP, Cui SW, Wang ZJ, Phillips AO, Phillips GO, et al. Structural characterization and immunostimulatory activity of a glucan from natural *Cordyceps sinensis*. Food Hydrocoll. 2017;67:139–47. https://doi.org/10.1016/j.foodhyd.2017.01.010.
36. Zhang Z, Guo L, Yan A, Feng L, Wan Y. Fractionation, structure and conformation characterization of polysaccharides from *Anoectochilus roxburghii*. Carbohydr Polym. 2020;231:115688. https://doi.org/10.1016/j.carbpol.2019.115688.
37. Yang X, Wei S, Lu X, Qiao X, Simal-Gandara J, Capanoglu E, et al. A neutral polysaccharide with a triple helix structure from ginger: characterization and immunomodulatory activity. Food Chem. 2021;350:129261. https://doi.org/10.1016/j.foodchem.2021.129261.
38. Zhang XM, Liao WF, Cong QF, Dong Q, Ding K. Isolation and structural characterization of the polysaccharides of cortex mori radices. Acta Chim Sin. 2013;71:722–8. https://doi.org/10.6023/A13010109.
39. Wendehenne D, Pugin A, Klessig DF, Durner J. Nitric oxide: comparative synthesis and signaling in animal and plant cells. Trends Plant Sci. 2001;6(4):177–83. https://doi.org/10.1016/s1360-1385(01)01893-3.
40. Kashfi K, Kannikal J, Nath N. Macrophage reprogramming and cancer therapeutics: role of iNOS-Derived NO. Cells. 2021;10(11):3194. https://doi.org/10.3390/cells10113194.
41. Ryll R, Kumazawa Y, Yano I. Immunological properties of trehalose dimycolate (cord factor) and other mycolic acid-containing glycolipids—a review. Microbiol Immunol. 2001;45(12):801–11. https://doi.org/10.1111/j.1348-0421.2001.tb01319.x.
42. Ren L, Zhang J, Zhang TH. Immunomodulatory activities of polysaccharides from *Ganoderma* on immune effector cells. Food Chem. 2021;340:127933. https://doi.org/10.1016/j.foodchem.2020.127933.
43. Hwang J, Yadav D, Lee PCW, Jin JO. Immunomodulatory effects of polysaccharides from marine algae for treating cancer, infectious disease, and inflammation. Phytother Res. 2022;36(2):761–77. https://doi.org/10.1002/ptr.7348.
44. Zhao S, Gao Q, Rong CB, Wang SX, Zhao ZK, Liu Y, et al. Immunomodulatory effects of edible and medicinal mushrooms and their bioactive immunoregulatory products. J Fungi. 2020;6(4):269. https://doi.org/10.3390/jof6040269.
45. Wang YF, Zhang YF, Shao JJ, Ren XJ, Jia JX, Li BH. Study on the immunomodulatory activity of a novel polysaccharide from the lichen *Umbilicaria esculenta*. Int J Biol Macromol. 2019;121:846–51. https://doi.org/10.1016/j.ijbiomac.2018.10.080.
46. Zhang Y, Zeng Y, Men Y, Zhang JG, Liu HM, Sun YX. Structural characterization and immunomodulatory activity of exopolysaccharides from submerged culture of *Auricularia auricula*-judae. Int J Biol Macromol. 2018;115:978–84. https://doi.org/10.1016/j.ijbiomac.2018.04.145.
47. Wan XH, Yin YM, Zhou CZ, Hou L, Cui QH, Zhang XP, et al. Polysaccharides derived from Chinese medicinal herbs: a promising choice of vaccine adjuvants. Carbohydr Polym. 2022;276:118739. https://doi.org/10.1016/j.carbpol.2021.118739.
48. Wang DY, Liu YH, Zhao W. The adjuvant effects on vaccine and the immunomodulatory mechanisms of polysaccharides from traditional Chinese Medicine. Front Mol Biosci. 2021;8:655570. https://doi.org/10.3389/fmolb.2021.655570.
49. Fan SR, Wang YX, Zhang Y, Wu YM, Chen XM. *Achyranthes bidentata* polysaccharide activates nuclear factor-kappa B and promotes cytokine production in J774A.1 cells through TLR4/MyD88 signaling pathway. Front Pharmacol. 2021;12:753599. https://doi.org/10.3389/fphar.2021.753599.
50. Young ID, Nepogodiev SA, Black IM, Le Gall G, Wittmann A, Latousakis D, et al. Lipopolysaccharide associated with beta-2,6 fructan mediates TLR4-dependent immunomodulatory activity in vitro. Carbohydr Polym. 2022;277:118606. https://doi.org/10.1016/j.carbpol.2021.118606.
51. Mistry P, Laird MHW, Schwarz RS, Greene S, Dyson T, Snyder GA, et al. Inhibition of TLR2 signaling by small molecule inhibitors targeting a pocket within the TLR2 TIR domain. Proc Natl Acad Sci USA. 2015;112(17):5455–60. https://doi.org/10.1073/pnas.1422576112.
52. Jiang LJ, Xu ZX, Li H, Wu MF, Wang FD, Liu SY, et al. TAK-242 exerts a neuroprotective effect via suppression of the TLR4/MyD88/TRIF/NF-kappa B signaling pathway in a neonatal hypoxic-ischemic encephalopathy rat model. Mol Med Rep. 2020;22(2):1440–8. https://doi.org/10.3892/mmr.2020.11220.
53. Ono Y, Maejima Y, Saito M, Sakamoto K, Horita S, Shimomura K, et al. TAK-242, a specific inhibitor of Toll-like receptor 4 signalling, prevents endotoxemia-indfiuced skeletal muscle wasting in mice. Sci Rep-UK. 2020;10(1):694. https://doi.org/10.1038/s41598-020-57714-3.
54. Zhu LJ, Li W, Fan ZY, Ye XY, Lin RY, Ban MM, et al. Immunomodulatory activity of polysaccharide from *Arca granosa* Linnaeus via TLR4/MyD88/NF kappa B and TLR4/TRIF signaling pathways. J Funct Foods. 2021;84:104579. https://doi.org/10.1016/j.jff.2021.104579.

Publisher's Note